Power hardware-in-the-loop simulations of grid integration of a wave power park

Irina Temiz, Arvind Parwal, James Kelly, Tatiana Potapenko, Jennifer Leijon, Sara Anttila, Johannes Hjalmarsson, Laure Hebert, and Cecilia Boström

Abstract—**This paper describes experiments conducted at the Centre for Marine and Renewable Energy Ireland (MaREI) in Cork, Ireland. Integration of a single wave energy converter (WEC) and a wave power park (WPP) consisting of three and ten WECs in a (micro-) grid is studied in real time using the power hardware-in-the-loop (PHIL) equipment. Two different ways to emulate the output power from a WEC and a WPP are used. A single WEC is emulated using a squirrel cage induction generator (SCIG) run by a grid-powered motor. A hydrodynamic model of a point absorber with a permanent magnet synchronous generator is implemented in MATLAB/Simulink and used to emulate an irregular output power from a WEC. In the other case, a WPP is emulated using a Triphase power converter where the DC currents are injected at the DC-link of the converter. The time series of currents for the DC-link injection are based on data obtained in earlier offshore experiments conducted at the Lysekil research site, Sweden. To emulate a WPP, the experimental output currents from one WEC are replicated three and ten times, superimposed following different scenarios and rectified. The rectified currents are used as an input for the DC-link. Different scenarios of superimposing are considered covering the worst and the best case scenarios. Power fluctuations, interaction with the main grid and microgrid, load bank and batteries are studied for different wave conditions.**

Keywords— **energy storage system, grid integration, hardware-in-the-loop, microgrid, power fluctuations, wave energy converter, wave power, wave power park.**

I. Introduction

OCEAN waves contain a large amount of energy and researchers and engineers across the globe are seeking for an efficient way to harvest wave power and convert it to electrical power. Different devices have been invented and tested through the decades, see e.g. [1]–[3].

The wave energy converter (WEC) concept developed and studied at Uppsala University, Sweden (www.teknik.uu.se/electricity/), is a point absorber with a permanent magnet direct drive linear generator power take off (Fig. 1). The system is scalable and robust. With the current design parameters, each device can produce an output power up to 100 kW depending of the wave climate. A key aspect of generating a significant amount of power from the WECs at a specific site is to include several WECs in a wave power park (WPP) [4] (Fig. 2) and to interconnect them via a marine substation, as described in e.g. [5].

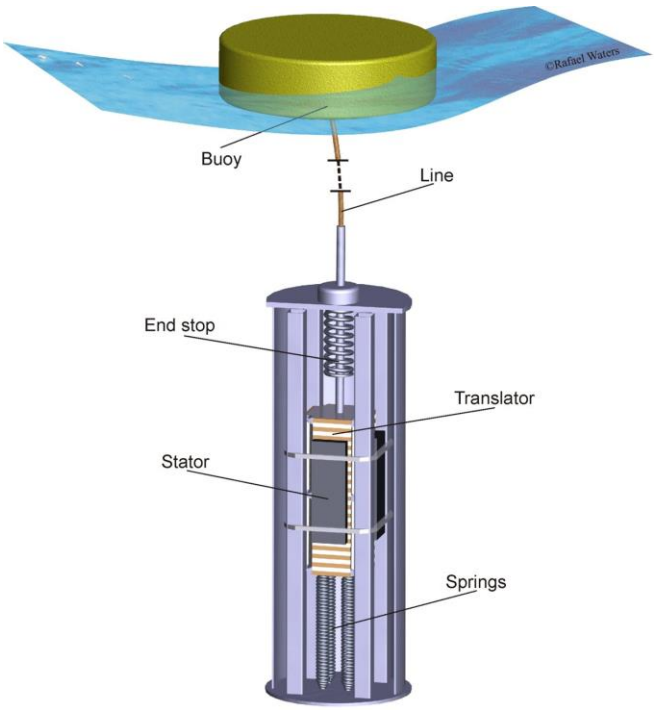

Fig. 1. Illustration of the wave energy converter.

The ID number of paper submission is 1596 and the conference track is GPC. This work was supported in part by Marinet2, SweGRIDS, StandUP for Energy, Swedish Research Council (VR) grant agreement No 2015-03126, Anna Maria Lundin foundation, Uppsala University, Miljöfonden, ÅForsk, J. Gust Richers foundation.

I. Temiz, A. Parwal, T. Potapenko, J. Leijon, S. Anttila, J. Hjalmarsson, and C. Boström are with Department of Engineering Sciences of Uppsala University, Box 534, Uppsala, 75121, Sweden (e-mail: irina.temiz@angstrom.uu.se, arvind.parwal@angstrom.uu.se, tatiana.potapenko@angstrom.uu.se, jennifer.leijon@angstrom.uu.se, sara.anttila@angstrom.uu.se, johannes.hjalmarsson@angstrom.uu.se, cecilia.bostrom@angstrom.uu.se).

J. Kelly is with MaREI, Centre for Marine and Renewable Energy Ireland, Beaufort Building, University College Cork, Ringaskiddy, Ireland (e-mail: james.kelly@ucc.ie).

L. Hebert was with Carl von Ossietzky Universität, Straße 9-11, 26129, Oldenburg, Germany and with Department of Engineering Sciences of Uppsala University, Box 534, Uppsala, Sweden (e-mail: hebertlaure@gmail.com).

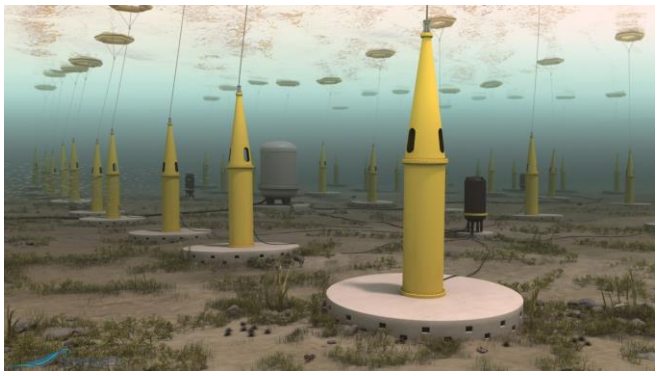

Fig. 2. Wave energy converters interconnected to a wave power park (courtesy of Seabased AB).

A. *Grid integration of WPPs*

Grid integration of variable power sources, particularly WPPs, is an ongoing research. Little is known about grid integration of WPPs.

Although several WEC concepts were tested offshore, only some of them were reported as grid connected, e.g. Pico plant in Portugal [6], LIMPET in UK [7], Wave Dragon in Denmark [8], Pelamis in Scotland [8]. To the authors' knowledge, there is no literature presenting experiments on grid connected WECs and WPPs. Cost and insecurity of performing full-scale experiments limits the availability of data from actual WPPs.

Nevertheless, the researchers investigate grid integration of WPPs numerically. Wave farms flickers severity was investigated for three different WEC concepts and different park configurations [9]. Impact of WPPs on power system frequency for islanded electrical systems was analysed and use of different energy storage systems was discussed in [10]. A control strategy for an energy storage system consisting of supercapacitors was proposed in [11]. A hybrid energy storage system comprising batteries and supercapacitors with fully active topology was studied in [12].

Since the step from computer simulations to offshore experiments or full WPP deployment and grid integration can be very large, other methods of grid integration emulation are beneficial, particularly, power hardware-in-the-loop (PHIL) can be used for this purpose.

B. *Power hardware-in-the-loop*

Hardware-in-the-loop (HIL) systems usually consist of a physical controller combined with a virtual plant executed in real-time (RT) computer simulations. RT simulations with HIL allow to test the controller at earlier development stages, to discover eventual design issues at different operational – including faulty and extreme – conditions, to replace risky and expensive physical tests and, thereby, to reduce the development costs [13].

PHIL systems have been widely utilized to study control strategies for grid integration of different renewable energy sources (RESs) to the grid. Within the wave energy field, PHIL was used to emulate output power of oscillating water columns [14], [15], heaving point absorbers [16], [17], an oscillating wave surge converter [18], and a two-raft-type wave energy converter [19]. The methodology of integration of a WEC into electrical infrastructure, challenges and limitations were discussed in [20].

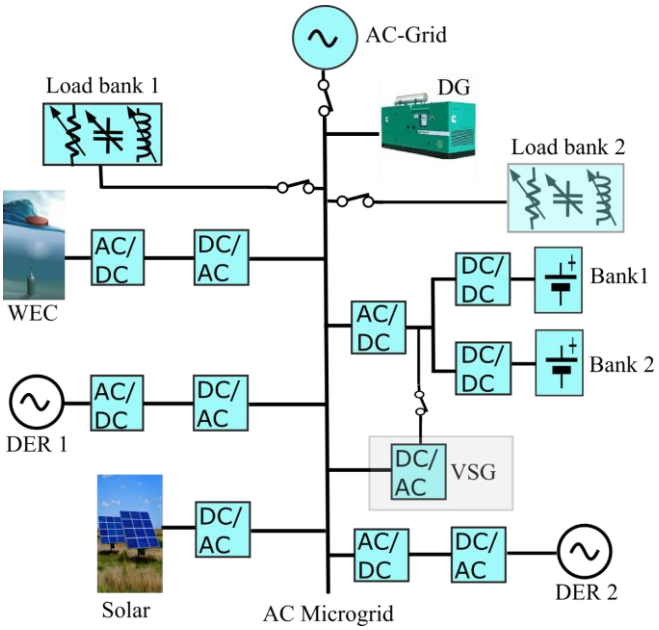

Fig. 3. Structure of the microgrid at UCC, MaREI facility.

C. *Article outline*

This paper describes the experiments conducted at the Centre for Marine and Renewable Energy Ireland (MaREI, www.lir-notf.com/electricallaboratory) in Cork, Ireland, in October 2018. The study is carried out to demonstrate the behaviour of an intermittent power source – a single WEC and WPPs – with the AC-microgrid and to test the effectiveness of the proposed virtual synchronous generator (VSG) control algorithms.

The rest of the paper is organized as follows. Firstly, the testing setup at MaREI is shortly described. Secondly, input to the PHIL equipment emulating performance of a single WEC and WPPs is presented. Thirdly, conducted experiments are outlined, and finally, challenges and limitations of performed experiments are indicated.

II. Experimental Setup

The Power Hardware-in-the-Loop (PHIL) experiments presented in this paper were conducted at electrical laboratory of the Lir National Ocean Test Facility (NOTF) at the MaREI Centre in University College Cork (UCC), Ireland. A detailed description of the PHIL system is given in [21]. The microgrid setup running at 400 VAC line-line RMS voltage is shown in Fig. 3.

The electrical laboratory includes a microgrid that consists of a dual-bus three phase system. Generation, storage and load elements can be added to the microgrid to build up an extensive variety of test configurations. The microgrid can be operated in parallel with local grid or as an islanded system. Sources of power include a 33 kVA diesel generator, a wind/ocean energy emulator, and fully controllable Triphase back-to-back 90 kW and 15 kW convert-

Fig. 4. The rotatory emulator connected to the microgrid.

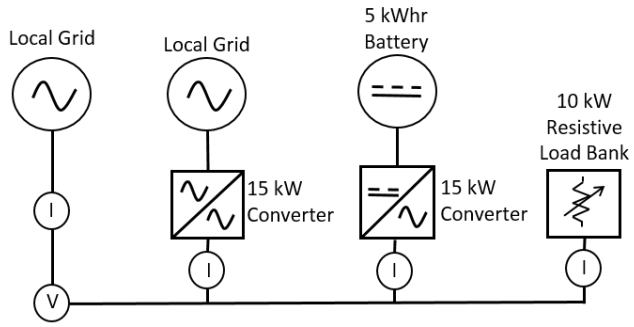

Fig. 5. Single line diagram of experimental configuration.

ers that can exchange power between the grid and microgrid offering excellent experimental flexibility. Storage is provided by a 5 kWh lithium ion battery with 10 kW peak power flows, which is controlled by one of the 15 kW back-to-back converters. Full controllable and adjustable loads with leading and lagging power factors are available including a 50 kVA Crestchic loadbank. Robust system control is provided by industry standard PLCs, while high speed data acquisition is offered by National Instruments cRIO system. An Opal-RT PHIL system OP5600 provides advanced grid specific grid emulation capabilities.

The wind/ocean energy emulator (Fig. 4) consists of two directly coupled electrical machines: a prime mover, acting as a WEC, and the other acting as the rotatory generator. The generator is connected to the microgrid using a back-to-back power converter topology. The real-time simulator uses MATLAB/ Simulink to interact directly with the emulator, allowing for more accurate and complex modelling. The control algorithms were executed in the PHIL connected to the PC.

The microgrid was developed with an extensive SCADA system, which allows for high frequency sampling of the electrical power flow. The SCADA system includes voltage transducers for all three phases for both buses of the microgrid. In addition to the voltage transducers, each individual device attached to the microgrid, including the local grid connection, has current transducers for each phase. Fig. 5 shows a single line diagram for configuration of the microgrid as applied for the experiments presented here, this includes the voltage and current transducers.

The system is controlled by the National Instruments (NI) cRIO and allows for sampling frequencies of up to 40 kHz. The ability to sample the current and voltage transducers at such high frequencies permits full waveforms detection via data collected. By gathering full waveform electrical data, investigations of active and reactive power as well as total harmonic distortion and induced flicker can be applied to the experimental data. The experiments presented in this paper included a sampling frequency of 10 kHz, which was the maximum frequency that could be applied due to the large number of signals being sampled simultaneously.

III. INPUT TO PHIL

Two types of experiments were conducted and, therefore, two types of input data to the PHIL were used. One set of experiments was based on a hydrodynamic model of a single point absorber as described in Section D. In the other set of experiments, a power flow from a WPP was determined from experimental data obtained in offshore experiments in Lysekil, Sweden. The input data to the second set of experiments is described in Section E.

D. WEC hydrodynamic model

The WEC motion in heave is described by two equations [22]:

$$m_b \ddot{z}_b = F_e - F_r - F_h - F_{gb} + F_b - F_w \quad (1)$$

$$m_t \ddot{z}_t = F_w - F_d - F_{gt} - F_{es} - F_s \quad (2)$$

where m_b and m_t are the buoy and translator mass respectively, z_b and z_t are the buoy and translator displacements, F_e is the excitation force, F_r is the radiation force, F_h is the hydrostatic stiffness force, F_{gb} and F_{gt} are the gravity forces of the buoy and the translator respectively, F_b is the buoyancy force, F_w is the wire force used for coupling between the buoy and the translator motion, F_d is the electromagnetic damping force, F_{es} is the end stop spring force, and F_s is the retraction spring force. More detailed definition of forces acting on the WEC are given below and can be grouped as forces acting on the buoy and forces acting on the translator (Fig. 6). Friction force is neglected in this model, and connecting wire is assumed to be non-sagging and well stretched.

1) Forces on the buoy

The excitation and radiation forces are dependent on the amplitude and frequency of the incident wave and calculated from hydrodynamic coefficients obtained by means of WAMIT [23], a package software based on the potential linear flow theory.

In the time domain, the excitation force is given as a convolution of the impulse response function (IRF) of the excitation force $\hat{f}_e(t)$ and the water surface elevation at the given point $\eta(t)$.

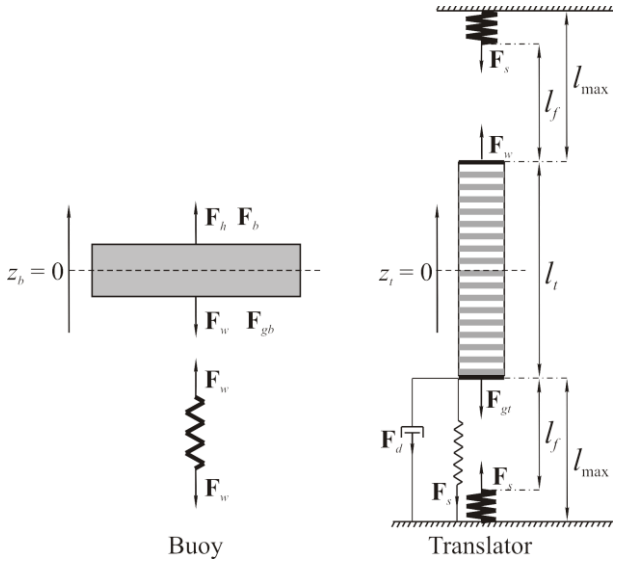

Fig. 6. Illustration of forces acting on the buoy and translator [22].

$$F_e(t) = \hat{f}_e(t) * \eta(t) \tag{3}$$

For a regular wave $\eta(t) = A\sin(\omega t)$ with the amplitude A and the angular frequency ω, the excitation force is given by

$$F_e(t) = \left|\hat{F}_e(\omega)\right| \cdot A\sin\left(\omega t + \phi_e(\omega)\right) \tag{4}$$

where $\left|\hat{F}_e(\omega)\right|$ and $\phi_e(\omega)$ are the amplitude and the phase of the excitation force coefficients at the given wave frequency ω.

The radiation force in time domain is found from

$$F_r(t) = m_a(\infty)\ddot{z}_b(t) + \hat{f}_r(t) * \dot{z}_b(t) \tag{5}$$

where $m_a(\infty)$ is the added mass at infinite frequency and $\hat{f}_r(t)$ is the IRF of the radiation.

The hydrostatic stiffness force is obtained as follows:

$$F_h(t) = c \cdot z_b(t) \tag{6}$$

where c is the hydrostatic stiffness coefficient.

The buoy gravity and buoyancy forces are constant forces given by $F_{gb} = m_b g$ and $F_b = \rho g \nabla$ respectively, where g is the gravitational acceleration, ρ is the sea water density and ∇ is the volume of the submerged part of the buoy.

The wire force F_w is modelled as a very stiff spring that can also slack if the buoy displacement is greater than the translator displacement.

$$F_w(t) = \begin{cases} k_w(z_b - z_t), & \text{if } z_b > z_t \\ 0, & \text{otherwise} \end{cases} \tag{7}$$

where k_w is the wire spring coefficient. The wire force couples the motion of the buoy and translator.

TABLE I
INPUT PARAMETERS TO A HYDRO-MECHANICAL MODEL [24]

Symbol	Quantity	Value
m_b	Buoy mass	2000 kg
m_t	Translator mass	1200 kg
R	Buoy radius	1.5 m
k_w	Wire spring coefficient	833 kN/m
k_s	Retractive spring coefficient	6.2 kN/m
F_0	Pre-tension of retractive spring	8.12 kN
l_u	Distance to the upper end stop spring	0.907 m
k_u	Upper end stop spring coefficient	238 kN/m
l_l	Distance to the lower end stop spring	0.890 m
k_l	Lower end stop spring coefficient	211 kN/m
γ	Damping force coefficient	50 kNs/m

2) Forces on the translator

The damping force is determined as a viscous damping with a constant coefficient γ and the impact of varying active area [24] was neglected.

$$F_d(t) = \gamma \cdot \dot{z}_t(t) \tag{8}$$

The damping coefficient γ was optimized for each tested wave.

The translator gravity force is given $F_{gt} = m_t g$.

The end stop forces are modelled as spring forces acting only when the translator only when the translator touches either of the end stop springs.

$$F_{es}(t) = \begin{cases} k_u(z_t - l_u), \text{if } z_t > l_u, \\ k_l(z_t + l_l), \text{if } z_t < -l_l, \\ 0, \qquad \text{otherwise} \end{cases} \tag{9}$$

where k_u and k_l are the spring coefficients of upper and lower end stops, and l_u and l_l are the distances to the upper and lower end stop springs, respectively.

The retraction spring force is defined by

$$F_s(t) = F_0 + k_s z_t \tag{10}$$

where F_0 is the pretension applied to the spring and k_s is the retractive spring coefficient.

Input parameters to the hydrodynamic model are given in Table I.

3) Linear to rotational motion transform

The electrical generator for the RT simulator at the MaREI is a squirrel-cage induction generator (SCIG). It is brought into rotation by means of a rotary rig. To imitate a linear generator motion with the SCIG, a variable torque was applied to the rotary rid. Similar to the method described in [25], the reciprocal velocity of the translator in the linear generator was converted to a unidirectional angular velocity of the SCIG varying within allowable limits of the rotary rig. An example of this transform is plotted in Fig. 7.

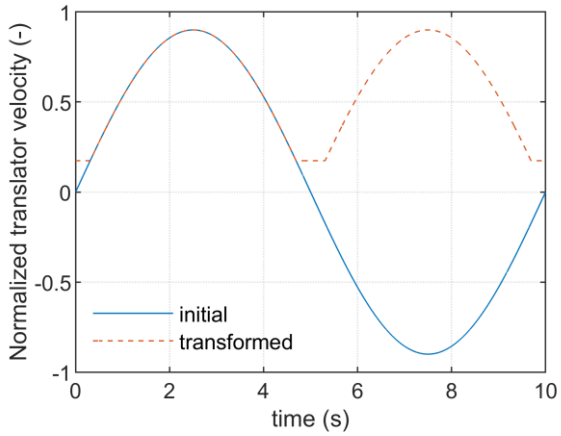

Fig. 7. Example of the reciprocal translator motion conversion to the rotational motion of SCIG plotted over a period of 10 s.

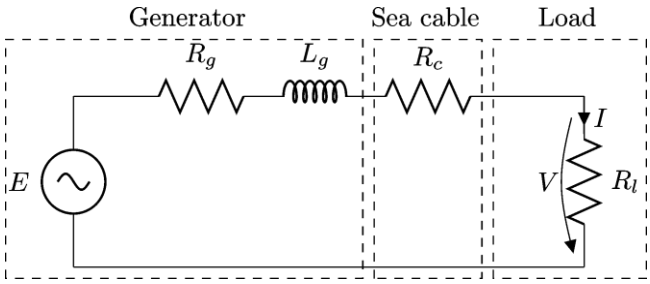

Fig. 8. A single line electric circuit diagram of the generator L9 connected via the subsea cable to a resistive load. I is the line current through the load and V is the line-to-neutral voltage across the load.

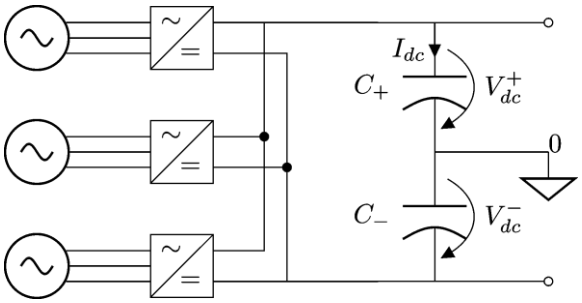

Fig. 9. An electrical layout of a wave power park consisting of three WECs. Currents from each WEC are rectified using diode rectifiers and connected to a common DC-link. A similar electrical layout was used for a wave power park consisting of ten WECs.

E. Experimental input data

The second set of input data was obtained using the output power data from a WEC during offshore experiments conducted in 2010 [26]–[28]. The offshore experiments were carried out at the Lysekil test site located on the west coast of Sweden. The WEC used in the experiments consisted of a torus-shaped point absorbing buoy connected via a stiff wire to the translator of a linear generator (called L9). Parameters of the generator L9 and the sea cable resistance are given in Table II [29]. The buoy consisted of six tubular sections of a length of 3 m. The volume of the buoy was 13.4 m^3 and the buoy weight was 3500 kg.

The WEC was connected to different delta-connected resistive loads equivalent to Y-connected resistances of 4.95 Ω, 11 Ω, and 27 Ω. Line-to-neutral voltages V_{abc} and

TABLE II
PARAMETERS OF THE GENERATOR L9 [29]

Symbol	Quantity	Value
V	Voltage [a,b]	450 V
P	Nominal power [b]	20 kW
R_g	Generator resistance	1 Ω
L_g	Generator inductance	20 mH
R_c	Cable resistance	0.54 Ω
R_l	Load resistance [c]	4.95 Ω, 11 Ω, and 27 Ω

[a] RMS line-to-line voltage
[b] at the translator speed of 0.7 m/s
[c] Y-connected equivalent resistance

line currents I_{abc} were measured onshore with sampling frequency of 256 Hz and saved in 60 s time series. For microgrid experiments at UCC, the induced no-load voltages E_{abc} were calculated from V_{abc} using the single line diagram (Fig. 8) and then used to obtain rectified voltage V_{dc} and current I_{dc} (Fig. 9) to be injected at the DC-link of the power converter during the tests at UCC.

The output power from one WEC is limited, therefore the output power from three and ten WECs was combined to emulate a power flow from a WPP. Since the goal with this set of experiments was to validate control algorithms for the midrogrid, we did not use any hydrodynamic model to determine the power flow from each WEC in the wave power park. Instead, we considered several different scenarios including the worst case scenario, the best case scenario and a number of intermediate scenarios. In the worst case scenario, we assumed the same instantaneous wave hitting all buoys at the same time, resulting in the overlap of the currents from each WEC and for the best case scenario the rectified currents flow to the DC-bus at different time instants resulting in a smoother power injection to the microgrid (see Fig. 10).

An increasing number of WECs can lead to output power smoothening but can have an opposite effect as well. For example, considering the best case scenario, an increasing number of WECs in a WPP leads to a smoother power output from the WPP. If the WPP consists of three WECs, the power variability for the given time period is approximately 39 %, then for the WPP consisting of ten WECs the power variability is about 24%, where the power variability is defined as a relative standard deviation. For the worst case scenario, an increased number of WECs implies, on contrary, an increased variability of the power output. It is around 74 % for the WPP of three WECs and around 79 % for the WPP of ten WECs.

The output voltage V_{dc} and current I_{dc} from the WPP varied in amplitude, while the microgrid as UCC operated at the constant 400 V AC. To determine the current control of the power converters of the microgrid, the power output of the DC simulations were used to determine the expected current output of the WP system if it were operating at 400 V AC through the basic power conversion Eq. (11).

$$I_{ac} = P_{dc}/V_{ac} \tag{11}$$

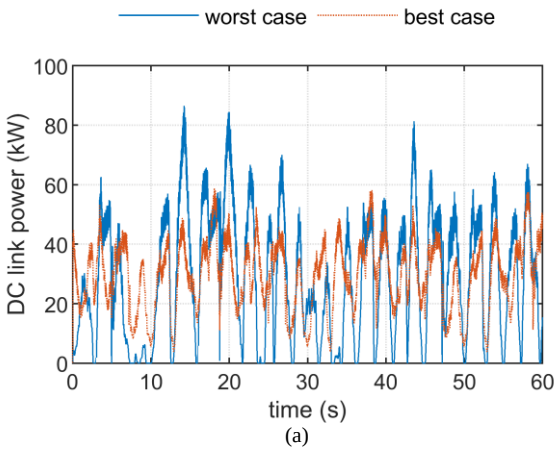

(a)

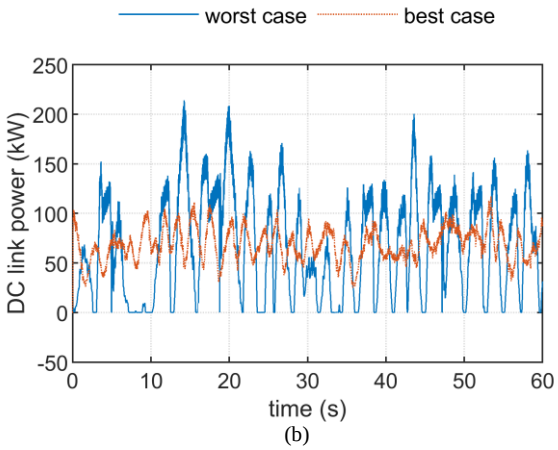

(b)

Fig. 10. An example of power P_{dc} at the DC-link for the best and worst case scenarios from a wave power park consisting of: (a) three WECs; (b) ten WECs.

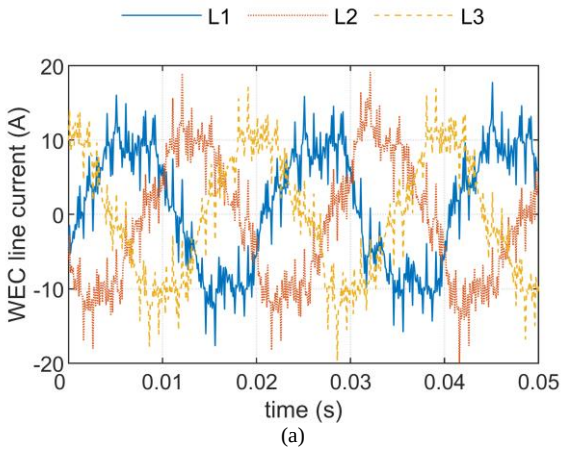

(a)

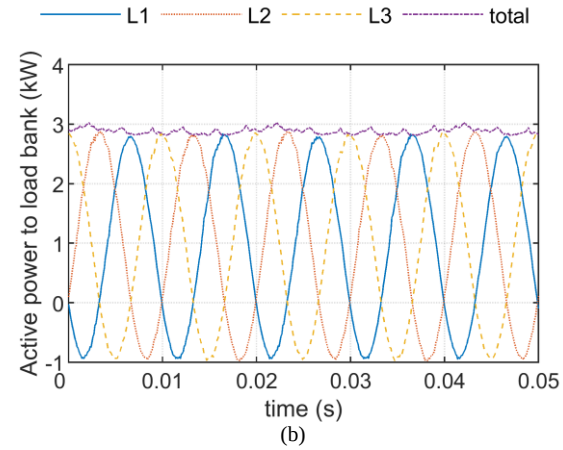

(b)

Fig. 11. Illustration the first category of experiments for the 0.8 m wave height and the 4.7 s wave period: (a) WEC output current; (b) active power delivered to the 5kW resistive load bank.

IV. RESULTS

F. *Single WEC interfaced with microgrid*

In the first category of experiments, a single WEC interfaced with microgrid was tested for different wave conditions. The ocean energy emulator was connected to the microgrid via a Triphase 15 kW back-to-back power converter in different topologies (grid, load, battery and the diesel generator).

The reference torque from the hydrodynamic model is used to control the motor speed and, hence, the rotatory generator. The speed limits of the motor are between 400 rpm to 2300 rpm. The generator is a SCIG machine and its stator is connected with the back-to-back power converter. An example of the WEC line currents operating under the wave conditions of 0.8 m wave height and 4.7 s wave period connected via the back-to-back converter to a resistive load bank is plotted in Fig. 11. The noisy signal of the WEC line currents in Fig. 11(a) is related to varying torque on the SCIG. The signals are output currents of SCIG before the inverter. Nevertheless, the signals displayed in Fig. 11(b) show that the proposed control scheme is able to control the output power flow to the load bank reasonably stable.

G. *RT simulations of WPPs*

The second category of experimentation operated in parallel with the local 3-phase, 400 V electrical grid, which operated as a strong grid that the WPP was supplementing. A Triphase 15 kW back-to-back power converter with active and reactive current control was used to emulate the WPP. Along with the WPP emulator, an electrical energy storage system was emulated with a second 15 kW back-to-back power converter that fed the lithium ion battery bank. The power converters were controlled using MATLAB/Simulink PHIL software developed by Triphase and customised by the engineers at UU and UCC. The configuration also included a local resistive load, which was adjusted to match the needs of each experimental run. The experiments were carried out for a duration of 60 seconds. Figs. 12 illustrates line currents from the WPP to the battery bank (BB) for WPPs consisting of three and ten WECs.

In the experiment, a control algorithm aiming to smooth out the output power from a WPP was applied. One can see the smoothen current from the WPP. However, no specific control on the BB was used, therefore, the current to the BB contains noticable harmonics and the harmonics content remains the same regardless of the number of WECs in the WPP. Comparing the current to the BB in Figs. 12 (a) and (b), it is obvious that the power flow from the

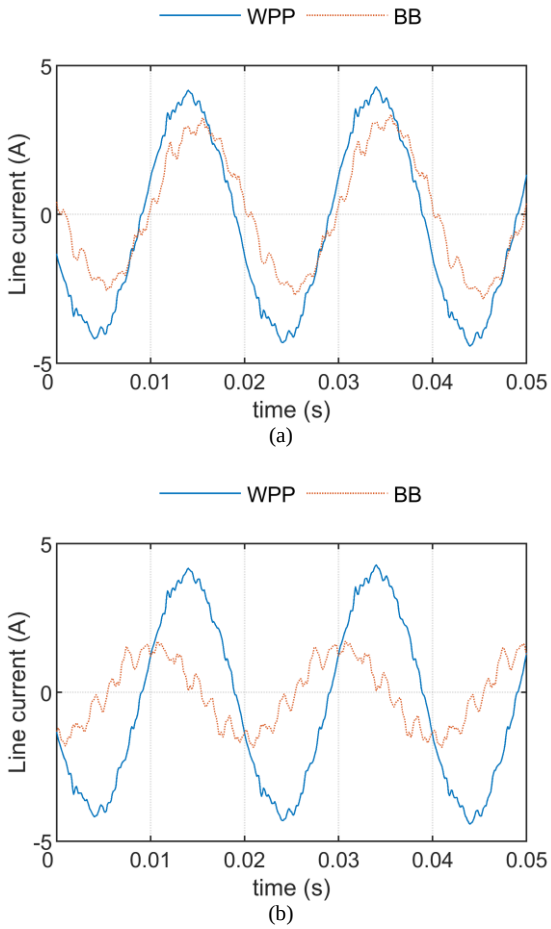

Fig. 12. Illustration the second category of experiments for the WPP consisting of: (a) 3 WECs; (b) 10 WECs.

WPP with ten WECs is smoother, as the current amplitude to the BB is less.

V. Discussion

Both sets of experiments were subject to a number of limitations.

Input into the PHIL comes from a mathematical model that shall always be validated. The validity of the model applied in the present study comes from earlier publications of UU's research group [24]. Implementation of the WEC damping force as a viscous damping does not fully reflect a nonlinear behaviour of the damping force as it is affected by the grid. In the future, an effective communication on the damping force between the ocean energy emulator and the WEC mathematical model shall also be used.

A linear generator behaviour differs from the behaviour of a rotational generator. Nevertheless, voltage and power fluctuations of the linear generator can be emulated with the variable speed rotational generator. These results are sufficient for validation of control algorithms.

Since experimental data was used in WPPs' RT simulations, the WEC output power depends on the design of the machine and the sea state. The WEC tested offshore was of an earlier design and was not fully optimized. Unfortunately, information about sea conditions for the moment when the offshore experiment was conducted is not available. On the other hand, it is well known that the wave climate at the Lysekil test site are mild and, therefore, a limited wave power can be absorbed.

In RT simulations with WPPs, the hydrodynamic interaction between WECs was not considered. It can be implemented in the future tests with WPPs containing even larger number of WECs. On the other hand, the hydrodynamic interaction between WECs is important for a collaborative control of each WEC in the WPP. In order to test, how the slowly varying output power from the WPP is injected to the grid, the assumptions made in the study are sufficient.

The collected data is used for control algorithms validation. The detailed algorithms and results can be found in [30], [31].

References

[1] J. Falnes, "A review of wave-energy extraction," *Mar. Struct.*, vol. 20, no. 4, pp. 185–201, 2007.

[2] A. F. de O. Falcão, "Wave energy utilization: A review of the technologies," *Renew. Sustain. Energy Rev.*, vol. 14, no. 3, pp. 899–918, 2010.

[3] D. Magagna, L. Margheritini, A. Alessi, E. Bannon, E. Boelman, D. Bould, V. Coy, E. De Marchi, P. Frigaard, C. Guedes Soares, C. Golightly, J. Hals Todalshaug, M. Heward, M. Hofmann, B. Holmes, C. Johnstone, Y. Kamizuru, T. Lewis, L. M. Macadre, C. Maisondieu, M. Martini, A. Moro, K. Nielsen, V. Reis, S. Robertson, P. Schild, M. Soede, N. Taylor, I. Viola, N. Wallet, X. Wadbled, and B. Yeats, *Workshop on identification of future emerging technologies in the ocean energy sector - 27th March 2018, Ispra, Italy*. Luxembourg: EUR 29315 EN, European Commission, 2018.

[4] M. Göteman, J. Engström, M. Eriksson, and J. Isberg, "Optimizing wave energy parks with over 1000 interacting point-absorbers using an approximate analytical method," *Int. J. Mar. Energy*, vol. 10, pp. 113–126, 2015.

[5] R. Ekström, A. Baudoine, M. Rahm, and M. Leijon, "Marine substation design for grid-connection of a research wave power plant on the Swedish West coast," in *Proc. of the 10th Eur. Wave and Tidal Energy Conf.*, 2013.

[6] A. Falcão, "The shoreline OWC wave power plant at the Azores," *Proc. fourth Eur. wave energy Conf.*, no. December, pp. 42–48, 2000.

[7] T. Heath, "Stuck on the Limpet," *Int. Water Power Dam Constr.*, vol. 51, no. 9, pp. 32–33, 1999.

[8] A. Westwood, "Ocean power: Wave and tidal energy review," *Refocus*, vol. 5, no. 5, pp. 50–55, 2004.

[9] T. Kovaltchouk, S. Armstrong, A. Blavette, H. Ben Ahmed, and B. Multon, "Wave farm flicker severity: Comparative analysis and solutions," *Renew. Energy*, vol. 91, pp. 32–39, 2016.

[10] J. I. Pérez-Díaz, D. Fernández, I. Villalba, M. Lafoz, M. Blanco, and F. Díaz, "Wave farms grid code compliance in isolated small power systems," *IET Renew. Power Gener.*, vol. 13, no. 1, pp. 171–179, 2018.

[11] L. P. Di Noia, A. Dannier, C. Pisani, A. Del Pizzo, and G. Brando, "Grid connection of wave energy converter in heaving mode operation by supercapacitor storage technology," *IET Renew. Power Gener.*, vol. 10, no. 1, pp. 88–97, 2015.

[12] A. Parwal, M. Fregelius, I. Temiz, M. Göteman, J. G. d. Oliveira, C. Boström, and M. Leijon, "Energy management for a grid-connected wave energy park through a hybrid energy storage system," *Appl. Energy*, vol. 231, no. April, pp.

399–411, 2018.

[13] J. Bélanger, P. Venne, and J.-N. Paquin, "The What, Where and Why of Real-Time Simulation," *Planet Rt*, vol. 1, no. 1, pp. 37–49, 2010.

[14] J. Kelly, D. O'Sullivan, W. M. D. Wright, R. Alcorn, and A. W. Lewis, "Challenges and lessons learned in the deployment of an offshore oscillating water column," in *COMPEL: The International Journal for Computation and Mathematics in Electrical and Electronic Engineering*, 2014, pp. 1678–1704.

[15] D. Ramirez, J. P. Bartolome, S. Martinez, L. C. Herrero, and M. Blanco, "Emulation of an OWC Ocean Energy Plant with PMSG and Irregular Wave Model," *IEEE Trans. Sustain. Energy*, vol. 6, no. 4, pp. 1515–1523, 2015.

[16] C. D. Signorelli, C. Villegas, and J. V. Ringwood, "Hardware-In-The-Loop Simulation of a Heaving Wave Energy Converter," in *Proceedings of the 9th European Wave and Tidal Energy Conference*, 2011, pp. 1–10.

[17] T. Hollis, H. B. Karayaka, Y.-H. Yu, and Y. Yan, "Hardware-in-the-Loop Simulation for the Proposed Slider-Crank Wave Energy Conversion Device," in *OCEANS 2018 MTS/IEEE Charleston*, 2019, pp. 1–7.

[18] S. Hazra, S. Bhattacharya, K. K. Uppalapati, and J. Bird, "Ocean energy power take-off using oscillating paddle," *2012 IEEE Energy Convers. Congr. Expo. ECCE 2012*, pp. 407–413, 2012.

[19] C. Liu, Q. Yang, and G. Bao, "Influence of hydraulic power take-off unit parameters on power capture ability of a two-raft-type wave energy converter," *Ocean Eng.*, vol. 150, no. November 2017, pp. 69–80, 2018.

[20] S. Armstrong, J. Rea, F. X. Faÿ, and E. Robles, "Lessons learned using electrical research test infrastructures to address the electrical challenges faced by ocean energy developers," *Int. J. Mar. Energy*, vol. 12, pp. 46–62, 2015.

[21] A. Monterrat, D. Murray, R. Christie, and J. Kelly, "Grid integration for marine renewable energy devices in a real time application," in *the 12th European Wave and Tidal Energy Conference (EWTEC17), 27th Aug -1st Sept 2017, Cork, Ireland*, 2017, pp. 1–7.

[22] I. Temiz, J. Leijon, B. Ekergård, and C. Boström, "Economic aspects of latching control for a wave energy converter with a direct drive linear generator power take-off," *Renew. Energy*, vol. 128, pp. 57–67, 2018.

[23] WAMIT, "User manual Version 7.0," *WAMIT, Inc.*, 2013. [Online]. Available: http://www.wamit.com/manual.htm. [Accessed: 16-Apr-2018].

[24] M. Eriksson, R. Waters, O. Svensson, J. Isberg, and M. Leijon, "Wave power absorption: Experiments in open sea and simulation," *J. Appl. Phys.*, vol. 102, no. 8, 2007.

[25] R. Ekström, S. Apelfröjd, and M. Leijon, "Experimental verifications of offshore marine substation for grid-connection of wave energy farm," *3rd Int. Conf. Electr. Power Energy Convers. Syst. EPECS 2013*, pp. 1–6, 2013.

[26] C. Boström, E. Lejerskog, S. Tyberg, O. Svensson, R. Waters, A. Savin, B. Bolund, M. Eriksson, and M. Leijon, "Experimental Results From an Offshore Wave Energy Converter," *J. Offshore Mech. Arct. Eng.*, vol. 132, pp. 041103-1-041103-5, 2010.

[27] E. Lejerskog, H. Gravråkmo, A. Savin, E. Strömstedt, S. Tyrberg, K. Haikonen, C. Boström, M. Rahman, R. Ekström, O. Svensson, J. Engström, B. Ekergård, A. Baudoin, V. Kurupath, L. Hai, W. Li, J. Sundberg, and M. Leijon, "Lysekil Research Site , Sweden : A Status Update," in *the 9th European Wave and Tidal Energy Conference, 5-9 September 2011, Southampton, UK*, 2011.

[28] E. Lejerskog, C. Boström, L. Hai, R. Waters, and M. Leijon, "Experimental results on power absorption from a wave energy converter at the Lysekil wave energy research site," *Renew. Energy*, vol. 77, pp. 9–14, 2015.

[29] Y. Hong, M. Eriksson, V. Castellucci, C. Boström, and R. Waters, "Linear generator-based wave energy converter model with experimental verification and three loading strategies," *IET Renew. Power Gener.*, vol. 10, no. 2, pp. 349–359, 2015.

[30] A. Parwal, M. Fregelius, D. C. Silva, T. Potapenko, J. Hjalmarsson, J. Kelly, I. Temiz, J. G. de Oliveira, C. Boström, and M. Leijon, "Virtual Synchronous Generator Based Current Synchronous Detection Scheme for a Virtual Inertia Emulation in SmartGrids," *Energy Power Eng.*, vol. 11, no. 03, pp. 99–131, 2019.

[31] A. Parwal, J. Hjalmarsson, T. Potapenko, S. Anttila, J. Leijon, J. Kelly, I. Temiz, J. G. de Oliveira, C. Boström, and M. Leijon, "Grid Impact and a Power Quality Assessment in Wave Energy Parks: Different Layouts and Power Penetrations using Energy Storage," *Submitt. to Int. J. Electr. Power Energy Syst.*, 2019.